

# Synthesis and cryogenic spectroscopy of narrow-diameter single-wall carbon nanotubes



Matthias S. Hofmann, Jonathan Noé, Manuel Nutz, Alexander Kneer, Raphael Dehmel, Lilian Schaffroth, Alexander Högele\*

Fakultät für Physik, Center for NanoScience (CeNS), and Munich Quantum Center, Ludwig-Maximilians-Universität München, Geschwister-Scholl-Platz 1, D-80539 München, Germany

## ARTICLE INFO

### Article history:

Received 7 March 2016

Received in revised form

15 April 2016

Accepted 28 April 2016

Available online 29 April 2016

## ABSTRACT

We report chemical vapor deposition and cryogenic photoluminescence studies of narrow-diameter single-wall carbon nanotubes. Our systematic study of synthesis parameters identifies means to control the average length, diameter, and areal density of carbon nanotubes grown on silica substrates. Using synthesis conditions that favor the growth of carbon nanotubes with sub-nanometer diameters, we fabricate samples with spatially isolated suspended nanotubes ideally suited for optical studies. Photoluminescence spectroscopy of individual nanotubes reveals two classes: spectrally broad and narrow single-peak emission at the temperature of liquid helium. The latter class with spectral line widths down to the resolution limit of our spectrometer of 40  $\mu\text{eV}$  indicates that exciton coherence in carbon nanotubes can be substantially improved by controlling the growth conditions and utilized in sources of indistinguishable single photons.

© 2016 The Author(s). Published by Elsevier Ltd. This is an open access article under the CC BY-NC-ND license (<http://creativecommons.org/licenses/by-nc-nd/4.0/>).

## 1. Introduction

Optical transitions of electron-hole pairs (excitons) [1,2] in semiconducting carbon nanotubes (CNTs) enable a wealth of potential optoelectronic applications [3] ranging from solar light harvesting devices [4] to single photon emitters [5] up to room temperature [6] for quantum cryptography and communication. In contrast to numerous studies of the optoelectronic properties of CNTs carried out on micelle-encapsulated nanotubes [7], reports on the photophysics of as-grown narrow-diameter CNTs with exciton photoluminescence (PL) at the lower wavelength edge of the CNT emission [8] have been sparse despite the technologically relevant window of silicon-based detectors with superior signal-to-noise performance, and the fundamental relevance of electron-hole Coulomb correlations that scale inversely with the nanotube diameter [9]. This is mainly owed to the facts that most synthesis methods for single-wall CNTs are neither chirality-selective nor do they yield abundant CNTs with sub-nanometer diameters and corresponding PL emission wavelengths below 1000 nm [8], and that non-suspended as-grown tubes in contact with the substrate

suffer from significant PL suppression [10].

The limited control of diameter-specific CNT growth is primarily a consequence of the complex interplay of the numerous synthesis parameters such as catalyst composition, size and pretreatment, carbon precursor, additives, temperature, or substrate support in catalytic chemical vapor deposition (CVD). Although this complexity has impeded a thorough microscopic understanding of the details involved in the CNT synthesis, remarkable progress has been achieved in the structural control of CNTs by means of catalyst design [11,12]. Variation of catalytic metals explored in other studies has indicated that single-wall CNTs with sub-nanometer diameters can be preferentially obtained under appropriate growth conditions [8,13–18]. Combined with the synthesis on structured substrates in the form of pillars [19] or trenches [10], samples with isolated as-grown narrow-diameter CNTs can thus be realized for fundamental studies of intrinsic optoelectronic properties [20] not compromised by side-wall wrapping molecular surfactants.

In the following, we present the results of our studies that aimed at realizing as-grown narrow-diameter CNTs isolated from the substrate for optical spectroscopy. We demonstrate how a significant fraction of CNTs with sub-nanometer diameters and PL emission wavelengths below 1000 nm can be obtained with optimized catalytic CVD synthesis. We investigated the impact of various CVD

\* Corresponding author.

E-mail address: [alexander.hoegel@lmu.de](mailto:alexander.hoegel@lmu.de) (A. Högele).

parameters on the nanotube lengths, diameters, and areal density, and employed an optimized synthesis method for the growth of individual narrow-diameter CNTs suspended on perforated membranes. PL spectroscopy of individual suspended nanotubes revealed two regimes of CNTs with single-peak emission at the temperature of liquid helium (4.2 K): in accord with previous studies we found CNTs with PL line widths in the range of a few millielectronvolts [21,22] and substantially below 1 meV [22,23] down to the resolution limit of our spectrometer.

## 2. Experimental

Our CVD process is based on methane in the presence of a bimetallic iron-ruthenium (FeRu) catalyst that has been reported to promote the growth of nanotubes with diameters of ~1 nm [15]. By choosing methane as the carbon feedstock for nanotube synthesis, amorphous carbon contamination is reduced due to its kinetic stability [24] and molecular decomposition is primarily assisted by the catalyst particles. Moreover, we used additional hydrogen gas which has been shown to promote the growth of clean CNT samples [25]. The FeRu catalyst was prepared from three stock solutions consisting of iron(III) nitrate nonahydrate ( $\text{Fe}(\text{NO}_3)_3 \cdot 9\text{H}_2\text{O}$ ), ruthenium(III) chloride hydrate ( $\text{RuCl}_3 \cdot x\text{H}_2\text{O}$ ), and alumina nanoparticles each dissolved in isopropyl alcohol. Concentrations of the stock solutions were chosen to be 4.65 g/l, 1.40 g/l, and 1.50 g/l, respectively. The solutions were stirred over night before small amounts were mixed together and diluted with isopropyl alcohol to obtain a catalyst solution with ingredient concentrations of 116.1 mg/l iron(III) nitrate nonahydrate, 35.0 mg/l ruthenium(III) chloride hydrate, and 37.5 mg/l alumina particles.

To control the areal density of the CNTs on silica, the solution was diluted further with isopropyl alcohol and bath-sonicated for 2 hours before its spin coating on the Si/SiO<sub>2</sub> substrate resulted in nanometer-sized catalytic particles on the surface. In selected cases we treated the catalyst particles with an oxygen plasma that was provided by a standard plasma etcher (LabAsh 100) operated at 2 torr and 55 W for 180 s prior to the CVD process.

For nanotube synthesis the samples were transferred into the middle of our CVD system consisting of a tubular furnace (Nabertherm R40/500/12-B170) and a quartz tube measuring 130 cm in length and 32 mm in inner diameter (wall thickness: 2 mm). The furnace was heated to a growth temperature in the range of 700–900 °C at a flow rate of 1.5 standard liters per minute (slm) of inert argon with 5% hydrogen. After reaching the growth temperature the CVD tube was flushed with hydrogen at 1.0 slm for 5 min to reduce the catalyst particles. Subsequently, methane and hydrogen with a fixed CH<sub>4</sub>/H<sub>2</sub> flow rate ratio of 1.33 were passed through the reaction chamber for carbon nanotube synthesis. Under these conditions the growth was maintained for 10 min. Afterwards the supply of CH<sub>4</sub> was stopped and the samples were gradually cooled in a hydrogen flow at 0.5 slm. At a temperature of ~500 °C hydrogen was replaced by argon with 5% hydrogen. Finally, the samples were unloaded at a furnace temperature of ~300 °C.

To obtain suspended CNTs we employed our CVD method on perforated silicon nitride substrates (DuraSiN Mesh for TEM, DTM-25233) with holes and craters 2 μm in diameter. To maintain the surface growth conditions of silica, the silicon nitride substrates were covered with a 100 nm thick layer of SiO<sub>2</sub> by plasma enhanced CVD (Oxford Instruments Plasmalab 80 Plus) prior to drop casting the catalyst solution onto the sample surface and subsequent blow-drying with nitrogen.

Carbon nanotube length and areal density data from CNTs on Si/SiO<sub>2</sub> was acquired by imaging the fabricated samples with a scanning electron microscope (Raith e\_Line) at an electron acceleration voltage of 0.7 keV. The CNT diameters were determined by height

profiling with tapping mode atomic force microscopy (AFM) (Digital Instruments Dimension 3100) under ambient conditions.

Cryogenic PL studies of individual CVD-grown CNTs were performed in a home-built confocal microscope in backscattering configuration at the temperature of liquid helium (4.2 K). The samples were positioned with respect to the excitation and detection spots of the microscope objective (Thorlabs C330TME-B) by a combination of nanometer-precise piezo steppers (attocube systems ANPxyz101) and scanners (attocube systems ANSxy100). Optical excitation was provided by a continuous wave titanium-sapphire laser (Coherent Mira900) at a fixed wavelength in the range of 730–850 nm. The PL of individual CNTs was filtered from laser background with a long-pass filter (Omega Optical 860AELP, cut-on at 860 nm), dispersed with a grating monochromator (Princeton Instruments Acton SP-2558) and recorded with a liquid nitrogen cooled low-noise silicon CCD (Princeton Instruments Spec-10:100BR/LN) with a lower detection limit of ~1.18 eV. The upper limit of the detection window was set by the long-pass filter to ~1.44 eV. By raster-scanning the sample with respect to the focal spot of the excitation laser and recording a PL spectrum at each displacement position we acquired spatio-spectral maps of individual sample regions with a spatial resolution of 1 μm and a spectrometer-limited spectral resolution of ~40 μeV.

## 3. Results

### 3.1. Influence of the synthesis parameters on carbon nanotube growth

Fig. 1a shows a representative scanning electron microscopy (SEM) image of CNTs grown on a Si/SiO<sub>2</sub> substrate. The growth temperature and the methane/hydrogen flow rate were 850 °C and 1.0 slm/0.75 slm, respectively. The median of 1.2 μm of the length distribution was extracted from a log-normal distributional fit to the data (Fig. 1b). We also studied the influence of the CVD temperature on the median length but found no significant dependence. However, similar to the results of Yang et al. [26], the nanotube lengths increased reproducibly by treating the deposited alumina-FeRu catalyst particles in an oxygen plasma prior to the CVD process. The increase was attributed to an immobilization of the catalyst particles on the support, thereby effectively suppressing particle coarsening and bulk diffusion [26], and enhancing the catalytic lifetime. Nanotubes with lengths of several tens of micrometers were obtained on oxygen plasma treated samples (SEM image in Fig. 1c). The evaluation of the acquired length distribution in Fig. 1d yielded a median of 2.9 μm, while the third quartile  $L_{Q3}$  increased from 1.9 μm for the untreated catalyst to 13.3 μm for the samples with catalyst treated by oxygen plasma. However, the obtained CNTs of a few ten micrometers in length are significantly bent (see Fig. 1c), supposedly due to the incorporation of carbon 5- and 7-rings into the CNT lattice [27]. The increased CNT average length was also accompanied by an increase of diameters and spectral line widths which will be discussed in more detail below.

In the next step, we investigated the influence of the synthesis temperature and the methane flow rate on the CNT density. To this end, we performed CNT synthesis on Si/SiO<sub>2</sub> substrates with a fixed concentration of the catalyst solution and temperatures between 700 and 850 °C (in steps of 50 °C) as well as for methane flows rates of 0.16, 0.37, 0.58, and 1.0 slm at a fixed methane/hydrogen flow rate ratio of 1.33. For each growth condition, several SEM images of equal sample areas were examined at random positions of the substrate and the CNT density was determined by CNT counting. The results are summarized in Fig. 2. The data points represent the mean density whereas the error bars give the highest and lowest densities determined from individual SEM images of a given

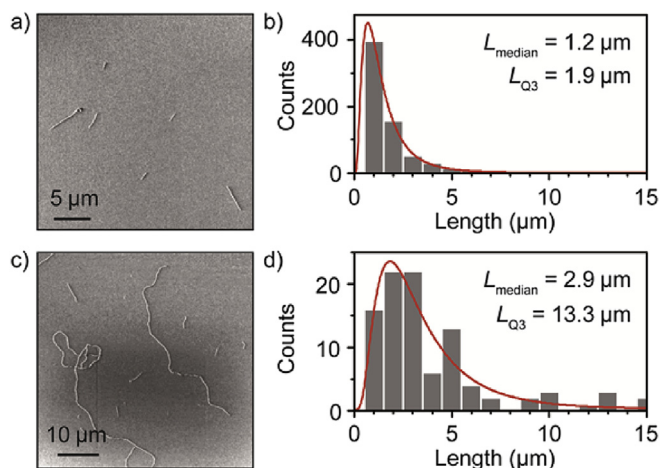


**Fig. 1.** Scanning electron micrographs of carbon nanotubes on a Si/SiO<sub>2</sub> substrate grown (a) without and (c) with oxygen plasma treatment of the catalyst particles prior to chemical vapor deposition. (b, d) The corresponding histograms with log-normal fits (red lines) show an increase in the median of the length distribution,  $L_{\text{median}}$ , as a result of catalyst treatment with oxygen plasma. The treatment facilitates growth of long carbon nanotubes indicated by the increase in the third quartile value,  $L_{Q3}$ . Note that the histogram in (d) does not show nanotubes with lengths above 15  $\mu\text{m}$  which were part of the statistical data analysis. (A color version of this figure can be viewed online.)

growth batch. We found that the methane flow rate did not influence the mean CNT density at a given temperature within the error of the data analysis (Fig. 2a). However, for a fixed methane flow rate, the CNT density increased significantly with increasing temperature up to 800 °C where it reached the point of saturation (Fig. 2b). These results indicate that our precursor/catalyst setup requires a certain thermal activation energy for efficient CNT growth. From the micrographs we found that many catalyst particles did not promote CNT growth at all. Therefore the saturation regime of the CNT areal density in Fig. 2b does not imply that all catalyst particles have been activated for nanotube synthesis. Low synthesis yield is a widely observed feature of catalytic CVD of CNTs. For instance, results from CNT growth with well separated Ni [28,29] or Fe [30] catalyst particles show a proportion of active catalyst particles below 20%. Such small CNT yields are most commonly attributed to the encapsulation of catalyst particles by graphitic shells as observed in high resolution transmission electron microscopy [31].

The CNT diameters were analyzed for synthesis temperatures of 750, 800, 850, and 900 °C, a methane flow rate of 1.0 slm at a methane/hydrogen flow rate ratio of 1.33, and without oxygen plasma treatment of the catalyst. Fig. 3a shows a representative AFM topography image of a (3.5 × 3.5)  $\mu\text{m}^2$  sample area with several catalyst particles and CNTs on the surface of the Si/SiO<sub>2</sub> substrate. The height profile along the dashed line was used to determine the diameters of three CNTs indicated by the arrows as 1.3 nm, 0.7 nm and 1.5 nm (Fig. 3b). To obtain statistics for the analysis of the nanotube diameter distributions resulting from different CVD parameters, this procedure was carried out at different sample areas. No statistically significant data were obtained for 700 °C since most catalyst particles remained inactive upon the variation of other growth parameters.

The results of the diameter analysis for the growth at the various temperatures are summarized in Fig. 3c. The median  $d_{\text{median}}$  of each diameter distribution was obtained from a log-normal fit (black lines in Fig. 3c) to the corresponding histogram. The values of  $d_{\text{median}}$  of 1.5, 1.1, and 1.0 nm at temperatures of 900, 850, and 800 °C, respectively, reveal a clear trend towards narrow-diameter CNTs with decreasing temperature. However, the distribution

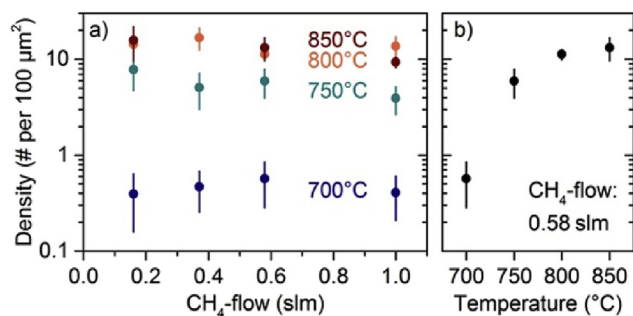


**Fig. 2.** (a) Carbon nanotube areal density on Si/SiO<sub>2</sub> substrate as a function of the methane supply rate in standard liters per minute (slm) at four temperatures (700, 750, 800, and 850 °C). The data points represent the mean density obtained from SEM image analysis for each temperature. Error bars indicate highest and lowest densities determined with SEM on different sample regions. For a given growth temperature the nanotube areal density is independent of the methane flow rate within the error of the data analysis. (b) Carbon nanotube areal density as a function of growth temperature for a methane flow rate of 0.58 slm. (A color version of this figure can be viewed online.)

median increased to 1.3 nm for 750 °C, suggesting a preference growth temperature around 800 °C for narrow-diameter CNTs with our CVD method. The diameter distribution was found to depend on the methane flow rate with variations of up to 20% in the median diameter for flow rates between 1.0 and 0.16 slm (data not shown) but without any statistically significant trend within the error bars of our analysis. We also investigated the diameter distributions on samples of the same CVD run with catalyst particles untreated and treated by oxygen plasma as described above and found that the catalyst pretreatment shifted the diameter distributions significantly towards larger values with a change in  $d_{\text{median}}$  by 0.8 nm for the case of CNT synthesis at 850 °C (Fig. 4). The increase in diameters also manifests in our PL studies in terms of increased emission wavelengths and line widths as will be described below.

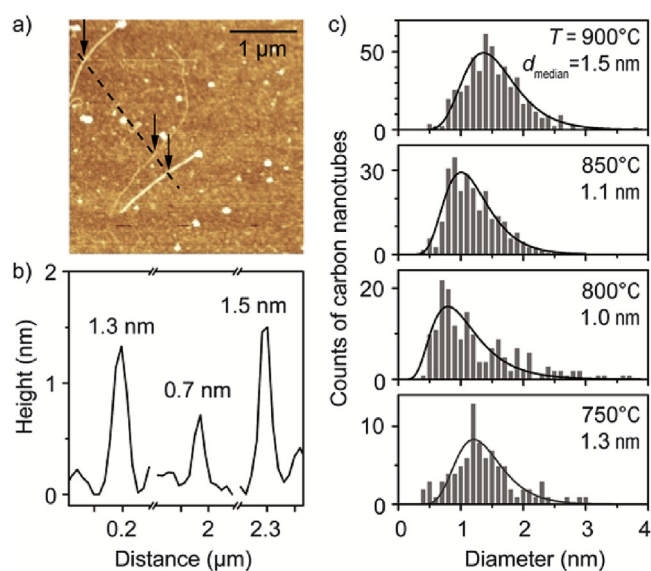


**Fig. 3.** (a) Atomic force micrograph of a (3.5 × 3.5)  $\mu\text{m}^2$  sample area with three as-grown carbon nanotubes. (b) Sections of the height profile along the dashed line in (a) yield diameters of 1.3, 0.7, and 1.5 nm for the nanotubes indicated by the arrows. (c) Diameter distributions of carbon nanotubes obtained for a methane flow rate of 1.0 slm and reaction temperatures of 900, 850, 800, and 750 °C (top to bottom) without catalyst pretreatment with oxygen plasma. The log-normal fits to the histograms (black lines) determine the median of the diameter distributions  $d_{\text{median}}$  given in the graphs. (A color version of this figure can be viewed online.)

### 3.2. Cryogenic spectroscopy of suspended narrow-diameter carbon nanotubes

In the following, we discuss cryogenic PL characteristics obtained for individual CNTs on two samples that differed in the treatment of catalyst particles prior to the CVD synthesis under identical growth conditions that were found to favor narrow-diameter CNTs. The sample without and with oxygen plasma treated catalyst will be termed in the following as sample A and B, respectively.

Our cryogenic experiments focused on the blue-most PL (above the cut-on of the long-pass filter) stemming from CNTs with the most narrow diameters by optimizing the chromatic collection optics of our setup around 900 nm. This experimental bias is probably enhanced even further by fixed laser wavelengths in the range of 730–850 nm that preferably address CNTs with higher emission energies through phonon-assisted excitation. Combined reflectance and spatio-spectral PL maps allowed us to locate individual suspended nanotubes on samples A and B as presented in Fig. 5a and c, respectively. The PL intensity maps (red-to-yellow color code) and the corresponding reflectance maps (black-to-white color code) in Fig. 5a and c identify nanotubes suspended over a crater and a hole, respectively. The reflectance and PL intensity map of Fig. 5c is complemented by a top layer of a semi-transparent SEM image of the same sample region. Only the left of the two CNTs indicated by the arrows was luminescent in our detection window. The corresponding spectral characteristics of the CNTs on samples A and B at 4.2 K are shown in Fig. 5b and d. Both samples featured CNTs with single symmetric resonances in the PL emission, however, with strikingly different line widths obtained from Lorentzian fits (red lines) to the data (gray circles). The full-width at half-maximum (FWHM) line width of the CNT in Fig. 5b was limited by the resolution of our spectrometer to 40  $\mu\text{eV}$ , a systematic feature of individual cryogenic CNT PL on sample A reported earlier [23] and other CNT samples obtained with our CVD growth under similar conditions. In contrast, the single-peak spectra of the CNTs on sample B were significantly broader, ranging from 1 to 10 meV at 4.2 K. Fig. 5d shows an example of such a broad and symmetric cryogenic spectrum of a suspended CNT with a FWHM line width of 6 meV. The observation of narrow and broad line widths as characteristic features of CNTs on sample A and B, respectively, is also reflected in the statistics of Fig. 6a: while the CNTs on sample A consistently exhibited narrow emission with line widths below 300  $\mu\text{eV}$ , the FWHMs of nanotubes on sample B scattered between 1 and 10 meV. The samples A and B differ not only in the FWHM distributions, sample B also lacks CNTs with most narrow diameters and PL emission energies above 1.35 eV (Fig. 6b). Although the distributions of the PL energies in the histograms of Fig. 6b from samples A and B have no one-to-one correspondence with the respective chirality [32,33] frequencies

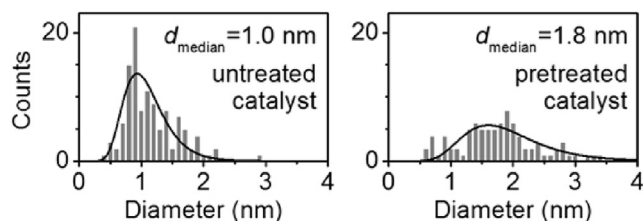


**Fig. 4.** Diameter distributions of carbon nanotubes obtained without (left panel) and with (right panel) catalyst treatment with oxygen plasma prior to carbon nanotube synthesis at a temperature of 850 °C and a methane flow rate of 1.0 slm. The medians of the diameter distributions  $d_{\text{median}}$  were determined by log-normal fits to the histograms (black lines).

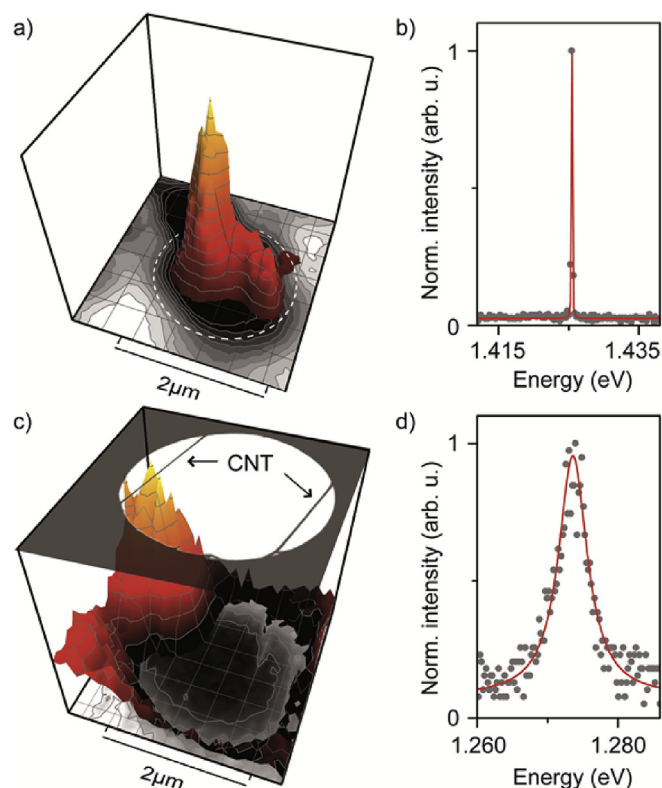


**Fig. 5.** (a) Combined raster-scan photoluminescence and reflectance maps (color-coded red-to-yellow and black-to-white, respectively) of a region on sample A with a carbon nanotube suspended over a crater (indicated by the dashed white circle). (b) Corresponding spectrum with a full-width at half-maximum line width of 40  $\mu\text{eV}$  limited by the spectrometer. (c) Raster-scan photoluminescence and reflectance maps of a hole on sample B complemented by a scanning electron micrograph (top layer) of two suspended carbon nanotubes (indicated by the arrows). (d) Spectrum of the photoluminescent nanotube in (c) with a line width of 6 meV. Red lines in (b) and (d) are Lorentzian fits to the spectra. Optical experiments were performed at 4.2 K. (A color version of this figure can be viewed online.)

because of our experimental bias to blue-most tubes, the trend towards larger diameters of CNTs obtained with oxygen plasma catalyst treatment on sample B found in AFM studies is clearly reflected by the statistics of the emission energies. For sample A, in contrast, the observation of emission energies above 1.35 eV is consistent with CNT diameters down to 0.6 nm in accord with our AFM results of Fig. 3.

Both regimes of broad and narrow PL emission from suspended CNTs of different chiralities have been reported in earlier studies of symmetric single-peak spectra with FWHM line widths in the range of a few millielectronvolts [21,22] and spectral narrow lines with FWHMs significantly below 1 meV at low temperatures [22,23]. However, a conclusive understanding of the processes that underlie the main difference of these regimes is still pending. In the framework of dephasing-limited PL line width and in absence of spectral fluctuations [22], the FWHM is a measure for the upper bound of exciton coherence by dephasing due to environmental inhomogeneities that are sampled by diffusive excitons during their lifetime [34]. Since localization inhibits exciton diffusion, one could argue on the basis of the PL energy distributions of CNTs on sample A and B (Fig. 6b) that narrow-diameter CNTs are more likely to exhibit narrow spectra (sample A) because they are more susceptible to fractionalization into quantum dots that localize excitons and protect them from decoherence at inhomogeneities encountered along the CNTs axis upon diffusion [23]. However,

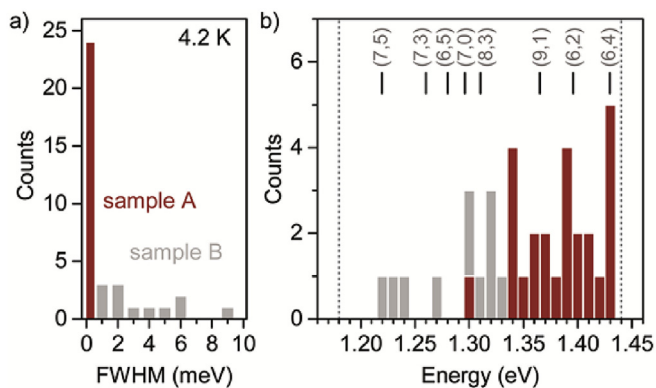


**Fig. 6.** (a) Histogram of the full-width at half-maximum (FWHM) line widths of single-peak photoluminescence spectra from individual suspended CNTs on samples A and B (red and gray bars, respectively) at 4.2 K. (b) Corresponding distribution of the photoluminescence peak energies of CNTs on sample A and B. Chirality-assigned emission energies at 4.2 K were calculated using room-temperature data of Ref. 32 and thermal band-gap renormalization according to Ref. 33, and are given on the top of the graph for reference. The upper and lower boundaries of our experimental detection window (dashed lines) are set by the cut-on of the long-pass filter at 860 nm (1.44 eV) and the sensitivity cut-off of the silicon CCD at  $\sim$ 1050 nm (1.18 eV), respectively. Note that the emission energy histograms do not reflect the chirality distribution of our CVD synthesis since nanotubes with highest emission energies were preferentially considered in our studies. (A color version of this figure can be viewed online.)

both classes of broad and narrow emission spectra have been reported for CNTs of the same chirality and similar emission energies, and have been attributed to the material quality rather than to exciton localization [22]. It is plausible that both exciton localization and environmental inhomogeneities at CNT side-walls play pivotal roles in determining the spectral characteristics of the CNT exciton PL. The individual contributions and their potential interplay, however, are to be substantiated in follow-up experiments on as-grown suspended CNTs with in-situ monitoring of a controlled cross-over from the diffusive to the localized exciton regime [35]. Ultimately, access to CNTs with spectrally narrow non-classical emission from localized excitons will represent a crucial step towards the realization of nanotube-based sources of indistinguishable photons [36].

#### 4. Conclusion

We presented a comprehensive study of a catalytic CVD method based on methane and FeRu-alumina catalyst particles that favors the growth of narrow-diameter CNTs under appropriate synthesis conditions. We used complementary analysis techniques to evaluate the effect of main synthesis parameters on the CNT average length, diameter and areal density. Using synthesis conditions that favor the growth of narrow-diameter CNTs, samples with suspended CNTs were fabricated and studied with cryogenic PL spectroscopy at 4.2 K. Comparative studies of suspended as-grown CNTs obtained with and without treatment of catalyst particles with oxygen plasma revealed two distinct regimes of CNT emission characterized by spectrally broad and narrow exciton PL. Spectral line widths as narrow as the resolution limit of our spectrometer indicate a timescale of  $\sim$ 15 ps as a lower bound for the exciton coherence in as-grown suspended CNTs at cryogenic temperatures.

#### Acknowledgements

We thank C. Schöenberger, M. Weiss, and A. Bachtold for their input on synthesis conditions, and P. Altpeter, R. Rath, and F. Storek for assistance in the clean room. This research was funded by the

European Research Council under the ERC Grant Agreement no. 336749, and the German Excellence Initiative via the Nanosystems Initiative Munich (NIM). We also acknowledge financial support from the Center for NanoScience (CeNS) and LMUinnovativ.

#### References

- [1] F. Wang, G. Dukovic, L.E. Brus, T.F. Heinz, The optical resonances in carbon nanotubes arise from excitons, *Science* 308 (2005) 838–841.
- [2] J. Maultzsch, R. Pomraenke, S. Reich, E. Chang, D. Prezzi, A. Ruini, et al., Exciton binding energies in carbon nanotubes from two-photon photoluminescence, *Phys. Rev. B* 72 (2005) 241402.
- [3] P. Avouris, M. Freitag, V. Perebeinos, Carbon-nanotube photonics and optoelectronics, *Nat. Photonics* 2 (2008) 341–350.
- [4] D.J. Bindl, M.-Y. Wu, F.C. Prehn, M.S. Arnold, Efficiently harvesting excitons from electronic type-controlled semiconducting carbon nanotube films, *Nano Lett.* 11 (2011) 455–460.
- [5] A. Högele, C. Galland, M. Winger, A. Imamoglu, Photon antibunching in the photoluminescence spectra of a single carbon nanotube, *Phys. Rev. Lett.* 100 (2008) 217401.
- [6] X. Ma, N.F. Hartmann, J.K.S. Baldwin, S.K. Doorn, H. Htoon, Room-temperature single-photon generation from solitary dopants of carbon nanotubes, *Nat. Nanotechnol.* 10 (2015) 671–675.
- [7] M.J. O'Connell, S.M. Bachilo, C.B. Huffman, V.C. Moore, M.S. Strano, E.H. Haroz, et al., Band gap fluorescence from individual single-walled carbon nanotubes, *Science* 297 (2002) 593–596.
- [8] S.M. Bachilo, L. Balzano, J.E. Herrera, F. Pompeo, D.E. Resasco, R.B. Weisman, Narrow (n, m)-distribution of single-walled carbon nanotubes grown using a solid supported catalyst, *J. Am. Chem. Soc.* 125 (2003) 11186–11187.
- [9] R.B. Capaz, C.D. Spataru, S. Ismail-Beigi, S.G. Louie, Diameter and chirality dependence of exciton properties in carbon nanotubes, *Phys. Rev. B* 74 (2006) 121401.
- [10] J. Lefebvre, D.G. Austing, J. Bond, P. Finnie, Photoluminescence imaging of suspended single-walled carbon nanotubes, *Nano Lett.* 6 (2006) 1603–1608.
- [11] F. Yang, X. Wang, D. Zhang, J. Yang, Da Luo, Z. Xu, et al., Chirality-specific growth of single-walled carbon nanotubes on solid alloy catalysts, *Nature* 510 (2014) 522–524.
- [12] J.R. Sanchez-Valencia, T. Dienel, O. Groning, I. Shorubalko, A. Mueller, M. Jansen, et al., Controlled synthesis of single-chirality carbon nanotubes, *Nature* 512 (2014) 61–64.
- [13] J. Kong, A.M. Cassell, H. Dai, Chemical vapor deposition of methane for single-walled carbon nanotubes, *Chem. Phys. Lett.* 292 (1998) 567–574.
- [14] L. An, J.M. Owens, L.E. McNeil, J. Liu, Synthesis of nearly uniform single-walled carbon nanotubes using identical metal-containing molecular nanoclusters as catalysts, *J. Am. Chem. Soc.* 124 (2002) 13688–13689.
- [15] X. Li, X. Tu, S. Zaric, K. Welsher, W.S. Seo, W. Zhao, et al., Selective synthesis combined with chemical separation of single-walled carbon nanotubes for chirality selection, *J. Am. Chem. Soc.* 129 (2007) 15770–15771.
- [16] W.-H. Chiang, R.M. Sankaran, Linking catalyst composition to chirality distributions of as-grown single-walled carbon nanotubes by tuning  $\text{Ni}_x\text{Fe}_{1-x}$  nanoparticles, *Nat. Mater.* 8 (2009) 882–886.
- [17] M. He, A.I. Chernov, P.V. Fedotov, E.D. Obratzsova, J. Sainio, E. Rikkinen, et al., Predominant (6,5) single-walled carbon nanotube growth on a copper-promoted iron catalyst, *J. Am. Chem. Soc.* 132 (2010) 13994–13996.
- [18] M. He, H. Jiang, B. Liu, P.V. Fedotov, A.I. Chernov, E.D. Obratzsova, et al., Chiral-selective growth of single-walled carbon nanotubes on lattice-mismatched epitaxial cobalt nanoparticles, *Sci. Rep.* 3 (2013) 1460.
- [19] A.M. Cassell, N.R. Franklin, T.W. Tomblor, E.M. Chan, J. Han, H. Dai, Directed growth of free-standing single-walled carbon nanotubes, *J. Am. Chem. Soc.* 121 (1999) 7975–7976.
- [20] Y. Homma, S. Chiashi, Y. Kobayashi, Suspended single-wall carbon nanotubes: synthesis and optical properties, *Rep. Prog. Phys.* 72 (2009) 066502.
- [21] J. Lefebvre, P. Finnie, Y. Homma, Temperature-dependent photoluminescence from single-walled carbon nanotubes, *Phys. Rev. B* 70 (2004) 045419.
- [22] I. Sarpkaya, Z. Zhang, W. Walden-Newman, X. Wang, J. Hone, C.W. Wong, et al., Prolonged spontaneous emission and dephasing of localized excitons in air-bridged carbon nanotubes, *Nat. Commun.* 4 (2013) 2152.
- [23] M.S. Hofmann, J.T. Glückert, J. Noé, C. Bourjau, R. Dehmel, A. Högele, Bright, long-lived and coherent excitons in carbon nanotube quantum dots, *Nat. Nanotechnol.* 8 (2013) 502–505.
- [24] J. Kong, H.T. Soh, A.M. Cassell, C.F. Quate, H. Dai, Synthesis of individual single-walled carbon nanotubes on patterned silicon wafers, *Nature* 395 (1998) 878–881.
- [25] A. Jungen, C. Stampfer, L. Durrer, T. Helbling, C. Hierold, Amorphous carbon contamination monitoring and process optimization for single-walled carbon nanotube integration, *Nanotechnology* 18 (2007) 075603.
- [26] J. Yang, S. Esconjauregui, R. Xie, H. Sugime, T. Makaryan, L. D'Arzié, et al., Effect of oxygen plasma alumina treatment on growth of carbon nanotube forests, *J. Phys. Chem. C* 118 (2014) 18683–18692.
- [27] R. Sharma, P. Rez, M. Brown, G. Du, M.M.J. Treacy, Dynamic observations of the effect of pressure and temperature conditions on the selective synthesis of carbon nanotubes, *Nanotechnology* 18 (2007) 125602.
- [28] M. Paillet, V. Jourdain, P. Poncharal, J.-L. Sauvajol, A. Zahab, J.C. Meyer, et al.,

- Versatile synthesis of individual single-walled carbon nanotubes from nickel nanoparticles for the study of their physical properties, *J. Phys. Chem. B* 108 (2004) 17112–17118.
- [29] M. Paillet, V. Jourdain, P. Poncharal, J.-L. Sauvajol, A. Zahab, J.C. Meyer, et al., Growth and physical properties of individual single-walled carbon nanotubes, *Diam. Relat. Mater.* 14 (2005) 1426–1431.
- [30] M. Ishida, H. Hongo, F. Nihey, Y. Ochiai, Diameter-controlled carbon nanotubes grown from lithographically defined nanoparticles, *Jpn. J. Appl. Phys.* 43 (2004) 1356.
- [31] M. Lin, J.P. Ying Tan, C. Boothroyd, K.P. Loh, E.S. Tok, Y.-L. Foo, Direct observation of single-walled carbon nanotube growth at the atomistic scale, *Nano Lett.* 6 (2006) 449–452.
- [32] R.B. Weisman, S.M. Bachilo, Dependence of optical transition energies on structure for single-walled carbon nanotubes in aqueous suspension: an empirical Kataura plot, *Nano Lett.* 3 (2003) 1235–1238.
- [33] R.B. Capaz, C.D. Spataru, P. Tangney, M.L. Cohen, S.G. Louie, Temperature dependence of the band gap of semiconducting carbon nanotubes, *Phys. Rev. Lett.* 94 (2005) 036801.
- [34] J.J. Crochet, J.G. Duque, J.H. Werner, B. Lounis, L. Cognet, S.K. Doorn, Disorder limited exciton transport in colloidal single-wall carbon nanotubes, *Nano Lett.* 12 (2012) 5091–5096.
- [35] X. Ma, O. Roslyak, J.G. Duque, X. Pang, S.K. Doorn, A. Piryatinski, et al., Influences of exciton diffusion and exciton-exciton annihilation on photon emission statistics of carbon nanotubes, *Phys. Rev. Lett.* 115 (2015) 017401.
- [36] C. Santori, D. Fattal, J. Vuckovic, G.S. Solomon, Y. Yamamoto, Indistinguishable photons from a single-photon device, *Nature* 419 (2002) 594–597.